ANNEALING EFFECT ON STRUCTURAL, OPTICAL AND ELECTRICAL PROPERTIES OF CdS THIN FILMS FOR PHOTOVOLTAIC APPLICATIONS

A. ALMOHAMMEDI[a], A. ASHOUR[a,b], E. R. SHAABAN[c]
[a]*Physics department, Faculty of Science, Islamic University, P. O. Box 170, Al Madinah, Saudi Arabia*
[b]*Physics department, Faculty of Science, Minia University, El Minia, Egypt*
[c]*Physics Department, Faculty of Science, Al–Azhar University, Assuit, 71542, Egypt*

CdS thin films with a thickness of 500 nm were prepared onto glass substrates by a thermal evaporation method. The effects of annealing temperature of CdS thin films were investigated at four different temperatures of 400, 500, 600 and 700 K for an hour in a nitrogen atmosphere. The crystallographic structure, the crystallite size and the lattice strain were studied by the X-ray diffraction pattern. The refractive indices and the film thickness have been evaluated in the transparent region using the envelope method in the transparent region. It was observed that the refractive index (n) decreases with increasing the film thickness**.** The band gap energy (E_g^{opt}) was identified and found to be decreased from 2.45 to 2.24 eV with increasing the annealing temperature. The electrical measurements by means of I-V measurement in dark and illumination condition and the electrical resistance were studied by using four probe method. The dark and photocurrents of the annealed CdS films were found to be greater than that of as deposited.

1. Introduction

Recently, cadmium sulphide thin films gained an extensive attention due to the promising applications in photovoltaic solar cells [1-4]. CdS is a n-type semiconductor and has a direct optical energy gap of about 2.45 eV, which recommend it as a window layer in solar cells. In addition, CdS has a high photosensitivity, thus it plays an important part of carrier generation in the photovoltaic solar cell [5, 6]. In CdS/CdTe solar cell, the light is penetrated and transmitted through the CdS layer to the p-type CdTe absorber layer and the photogenerated electron-hole pairs are divided in the depletion region of the CdS/CdTe heterojunction. The physical properties of the CdS layers can play an essential role in the performance and efficiency of CdS/CdTe solar cell [7, 8]. In terms of the crystal structure, CdS is solid hexagonal or cubic crystal.

Thermal annealing of CdS thin film is used to tune the structure, optical and electrical properties because the crystalline quality of the film plays an important role in the utilization of the CdS films for solar cell applications. The thermal annealing can improve the crystallinity of the films by removing the imperfections thus the strains, which can lead to improvements in both optical and electrical properties of the thin films. Sometimes, thermal annealing brings negative effects to CdS physical properties [2, 7-10], thus a better understanding of the influence of the annealed CdS film on the properties of the CdS/CdTe solar cell is still needed.

In this work, CdS films of 500 nm thickness were prepared by a thermal evaporation technique. Structural, morphological, optical and electrical properties of the deposited and

---

Corresponding author: esam_ramasan2008@yahoo.com

annealed CdS films were investigated. The photocurrents versus the applied voltage of the films are illuminated with a tungsten-halogen lamp of 500 W/m^2 output power. The changes in optical and electrical properties depending on annealing temperature are discussed in details and correlated with the changes in the structure parameters.

2. Experimental details

High purity (99.999%) CdS powder (Alrich chemicals company, USA) was evaporated from molybdenum boat to form the dielectric layer onto ultrasonically cleaned glass substrate kept at constant temperature (300 K), using a thermal evaporation unit (Denton Vacuum DV 502 A) and a vacuum of about 10^{-6} Pa. The substrate was rotated at a slow speed of 5 rpm to obtain a uniform CdS thin film. The deposition rate and the film thickness were controlled using a quartz crystal monitor DTM 100. The deposition rate was maintained at 20 Å/s during the sample preparations. The effects of annealing temperature on the 500 nm CdS thin films were investigated at four different temperatures (400, 500, 600 and 700 K) for an hour in a nitrogen atmosphere. After annealing, the films were left in a nitrogen atmosphere until temperature decreases to room temperature to avoid any oxidation of the film.

X-ray powder diffraction (XRD) using Philips diffractometry (model 1710), with Cu-K$_\alpha$ radiation (λ = 1.54056 Å) has been used to examine the phase purity and crystal structure of the as-deposited and annealed films. The elemental composition of the films was analyzed using energy dispersive X-ray spectrometer unit (EDXS). Moreover, scanning electron microscope (SEM model JOEL XL) with 30 kV was used to study the the film morphology. The relative error of determining the indicated elements does not exceed 2 %.

The transmittance (*T*) and reflectance (*R*) optical spectra of the deposited films were performed at room temperature using UV–VIS–NIR JASCO–670 double beam spectrophotometer. At normal incidence, the transmittance spectra were collected without a substrate in the reference beam in the wavelength range 300–2500 nm, while the reflectance spectra were measured using reflection attachment close to the normal incidence (~5°).

The electrical resistivity of the CdS thin films was measured at room temperature via measuring currents against applied voltage extended from 1 to 10 V using the four-probe technique. Indium coating was used as electrodes to make ohmic contacts to CdS layer. Before the dark measurement, the sample was maintained in dark for 12 h in order to empty all trapping states. The photocurrent versus the applied voltage of the as-deposited and annealed films was illuminated with a tungsten-halogen lamp with 500 W/m^2 output power.

3. Results and discussion

3.1. X-ray diffraction and morphological analysis

The effect of the thermal annealing on the structure of CdS film was investigated using the X-ray diffractogram as shown in Fig. 1. The XRD patterns exhibit polycrystalline phases of both as-deposited and annealed films. At low thermal annealing temperatures (400 and 500 K), all films show the presence of two crystalline phases cubic (C) phase (zinc blende-type, JCPDS 06-0314) and hexagonal (H) phase (wurtzite-type, JCPDS 10-0454) [11-16]. Thermal annealing leads to the increase of the intensity of the peaks due to the increase in the crystallinity of the film. At higher annealing temperatures (600 and 700 K), the hexagonal phase becomes dominating. The peak broadening is due to the instrumentation factor and structure factor that attributed to the crystallite size, the lattice strain.

Both crystallize size (*D*) and lattice strain *(e)* were determined using the Scherrer and Wilson equations [17, 18]:

$$D = \frac{0.9\lambda}{\beta\cos\theta} \tag{1}$$

$$e = \frac{\beta}{4 \tan \theta} \tag{2}$$

ehere β is the structural broadening that equals the difference in integral X-ray peak profile width which between the sample and the standard (silicon) and is given as: $\beta = \sqrt{\beta_{obs}^2 - \beta_{std}^2}$.
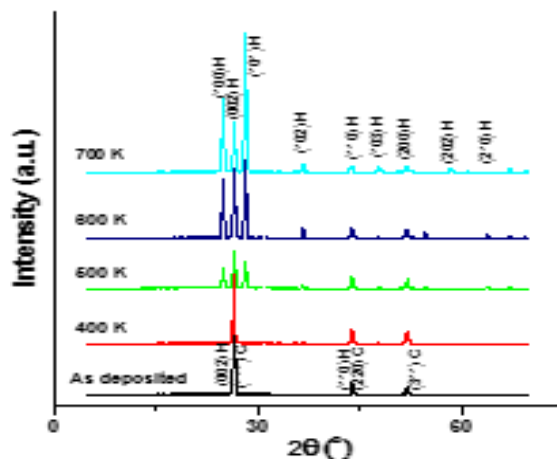
Fig. 1. X-ray diffractograms of the as-deposited and the annealed CdS thin films.

Fig. 2 shows the comparative look of microstructure parameters (D and e) of the CdS films of different annealing temperatures. It is observed that the average crystallite size increases with increasing the thermal annealing temperature (from 29 to 51 nm when the temperature increased from 300 to 700 K) but the lattice strain decreases (from 2×10^{-3} to 1.6×10^{-3} when the temperature increased from 300 to 700 K). Such a decrease in the lattice strain reflects the decrease in the concentration of lattice imperfections, which might be attributed to the decrease of breadth with increasing annealing temperature [19, 20]. The crystallize size was found to be lower than that reported by Metin et al. [21], which exhibit the crystallite size is 59 and 97 nm for as-deposited annealing at 723 K films, respectively. Such lower values of crystallize size may be attributed to the uniform film preparation by this method, which increases the broadening of the peaks [22, 23].

Furthermore, SEM measurement is very helpful to study the surface morphology of as-deposited film and those annealed at 500 and 700 K as shown in Fig. 3. It shows that the annealed uniformly distributed as a small cubic and hexagonal grains. Also, the results exhibit that the increase of the annealing temperature causes an increase in the size of the grains. The average particle size for as-deposited film and those annealed at 500 and 700 K was 22, 31 and 42 nm, respectively, revealed that its maximum dimension is always less than the crystallite size calculated from XRD data.

3.2. Optical properties

The transmission and reflection spectra of the as-deposited and annealed CdS thin films in the wavelength range of 300–2500 nm are shown in Fig. 4. At a higher wavelength of about 550 nm, all transmission of the films appears with fringes without shrinkage in amplitude particularly in medium absorption region, which indicates the homogenous structure of deposited CdS layers. Fig. 4 shows that the transmission of the films improves with increasing the annealing temperature. This improvement may be attributed to the reduction of lattice imperfections and voids inside the annealed films.
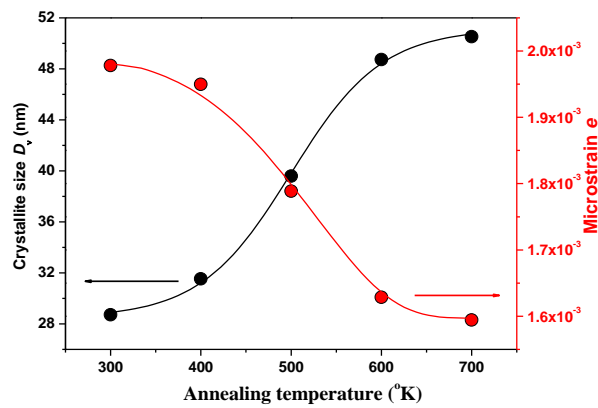
Fig. 2. Crystallite size and lattice strain versus annealing temperature of CdS films.
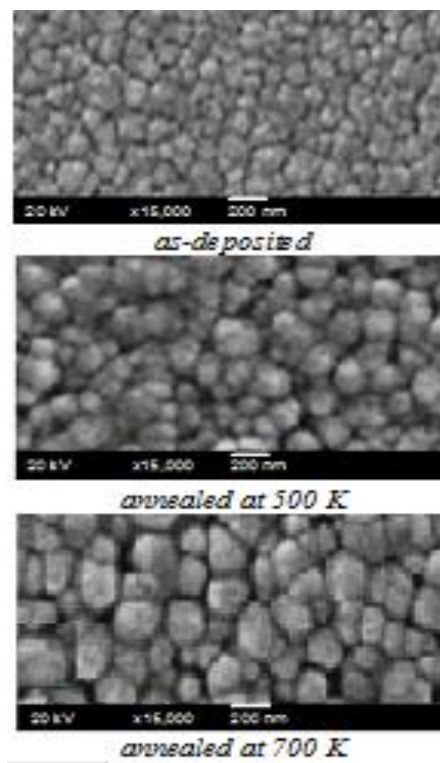
Fig. 3. SEM images of CdS thin films.

The absorption coefficient $\alpha(h\nu)$ can be obtained from the measured values of $R(\lambda)$ and $T(\lambda)$ in the strong absorption region from the following relationship [24, 25].

$$\alpha = \frac{1}{d}\ \ln\left[\frac{(1-R)^2 + \left[(1-R)^4 + 4R^2T^2\right]^{1/2}}{2T}\right] \qquad (3)$$

where d is the film thickness.

Fig. 5 shows the dependence of the absorption coefficient, α(*hv*) on the photon energy, *hv* as a function of annealed temperature. The absorption edge shifts toward lower energy region with increasing the annealing temperature. The optical energy gap of the films was determined in terms of the absorption coefficient, α(*hv*) using the Tauc formula [26, 27] as follows:

$$\alpha(h\upsilon) = \frac{K\,(h\upsilon - E_g^{opt})^{\frac{1}{2}}}{h\upsilon} \tag{4}$$
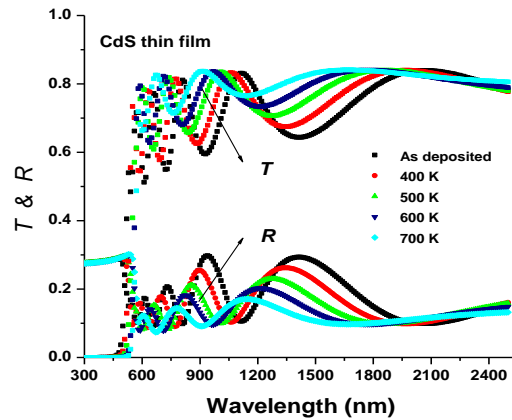
Fig. 4. Five typical transmission and reflection spectra of as-deposited and annealed CdS thin films.
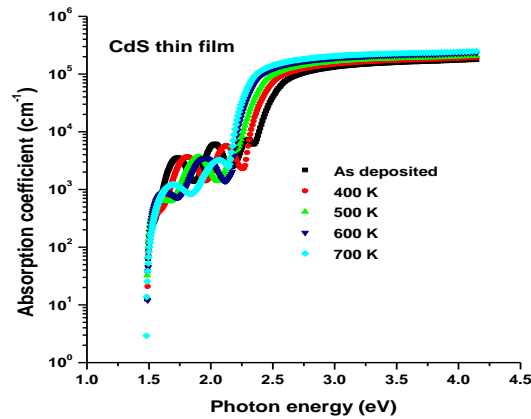
Fig. 5. Absorption coefficient against photon energy for as-deposited and annealed CdS thin films.

Fig. 6 shows the extrapolation of (α*hv*)² versus *hv* with the intercept of the straight line with the *hv* axis which gives the band gap values. The variation of energy gap (E_g^{opt}) versus the annealing temperature is shown in Fig. 7. The values of E_g^{opt} are found to be decreased from 2.45 to 2.24 eV when the annealing temperature increased from 300 to 700 K, respectively. The reduction in E_g^{opt} with increasing the annealing temperature may be attributed to the two reasons, the first is when the crystallite size increases the quantum confinement of electrons and holes decreases; consequently both the overlap factor between their wave functions and the absorption cross-section decrease, the second is the presence of trapping centers for electrons and holes due to

surface defects within the energy gap results in a strong interaction between the exciton and the trapped electron-hole pair-hence the bleaching of exciton absorption [28].
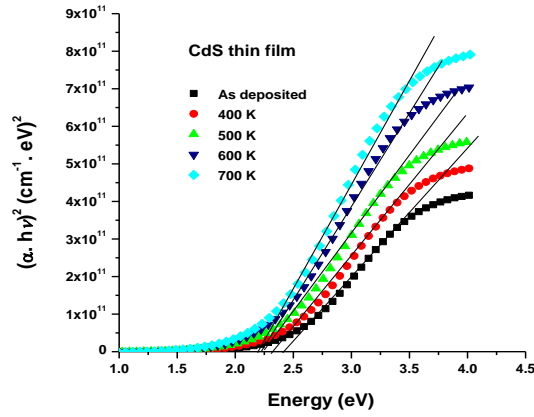
Fig. 6. Variations of $(\alpha h\nu)^2$ versus photon energy $(h\nu)$ for CdS films with different annealing temperatures.

According to the envelope method of transmission spectrum, the value of refractive index at a certain wavelength can be calculated using the following relationship [29-31]:

$$n = \left[N_1 + (N_1^2 - s^2)^{\frac{1}{2}} \right]^{\frac{1}{2}} \tag{5}$$

where

$$N_1 = 2s \frac{T_M - T_m}{T_M T_m} + \frac{s^2 + 1}{2} \tag{6}$$

where, T_M and T_m are the transmittance maximum and the corresponding minimum at a certain wavelength (λ) as shown in Fig. 8(a, b).
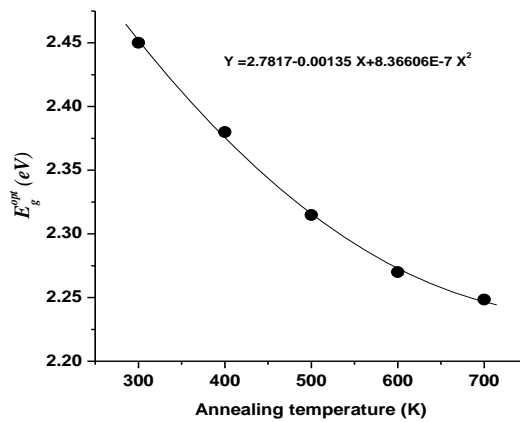
Fig. 7. Energy gap as a function of annealing temperature for CdS thin films.

The value of the refractive index of the substrate can be obtained from the transmittance spectrum of the substrate (T_s) using the well-known equation [31]:

$$s = \frac{1}{T_s} + (\frac{1}{T_s} - 1)^{\frac{1}{2}}$$

(7)

In terms of the calculated refractive indices n_l and n_2 at two adjacent maxima (or minima) at λ_1 and λ_2, respectively, the film thickness is given by the relationship

$$d = \frac{\lambda_1\lambda_2}{2(\lambda_1 n_{e2} - \lambda_2 n_{e1})}$$

(8)

The values of the film thickness of as-deposited and annealed CdS thin films was about $500 \pm 2\%$ nm. The refractive index of all films displays normal dispersion i.e. decrease with increasing wavelength (see Fig. 9) that follows Cauchy dispersion relationship, $n(\lambda) = a + b/\lambda^2$, which can be used for both interpolation and extrapolation over the whole wavelength. The least squares fit of the five sets of values of n corresponding the as-deposited and annealed yields $n = 2.24 + 2.24x10^5/\lambda^2$ for the as-deposited film, $n = 2.13 + 2.13x10^5/\lambda^2$ for annealing at 400 K, $n = 2.01 + 1.93x10^5/\lambda^2$ for annealing at 500 K, $n = 1.92 + 2.06x10^5/\lambda^2$ for annealing at 600 K and $n = 1.78 + 1.79x10^5/\lambda^2$ for annealing at 700 K. Fig. 9 shows that the refractive index decreases with increasing the thermal annealing temperature that may be attributed to the decrease in optical absorption, therefore the improvement in transmission spectra, thus the deviation of the light ray reduces, particularly in the visible region.
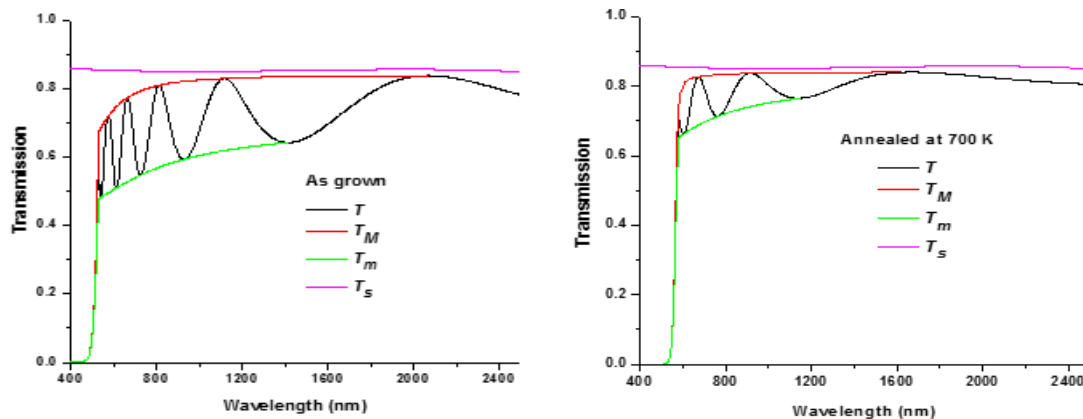
Fig. 8. The typical transmittance spectrum for CdS films thin film for as-deposited and annealed at 700 K.
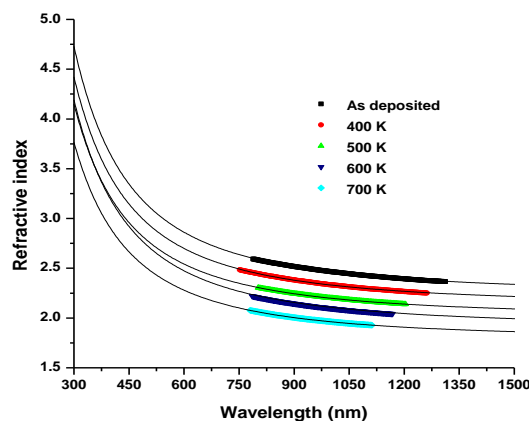
Fig. 9. The spectral dependence of refractive index (n) of CdS films with different annealing temperature.

3.3. Electrical properties

The I-V characteristic curves for the as-deposited and annealed CdS thin films were measured under darkness and illumination as shown in Fig 10. Fig. 10 (a, b) shows that both dark current and photocurrent increase with increasing the annealing temperature overall values of applied voltage. In addition, the photocurrent versus the applied voltage of each annealed film jump to higher values under the illumination. Fig. 11 (a, b) shows that the average resistance of the CdS films under dark and illumination as a function of thermal annealing temperature. As expected, the resistance decreases with the increase of the annealing temperature indicating semiconducting nature of the film. This behavior can be explained as follows: when annealing temperature increases, the crystallize size also increases, the grain boundaries decrease and hence the resistance is less. Under photo illumination, the photogenerated carriers get trapped at the grain boundaries, this reduces the inter-grain barrier height and carriers can move with less resistance [32, 33].
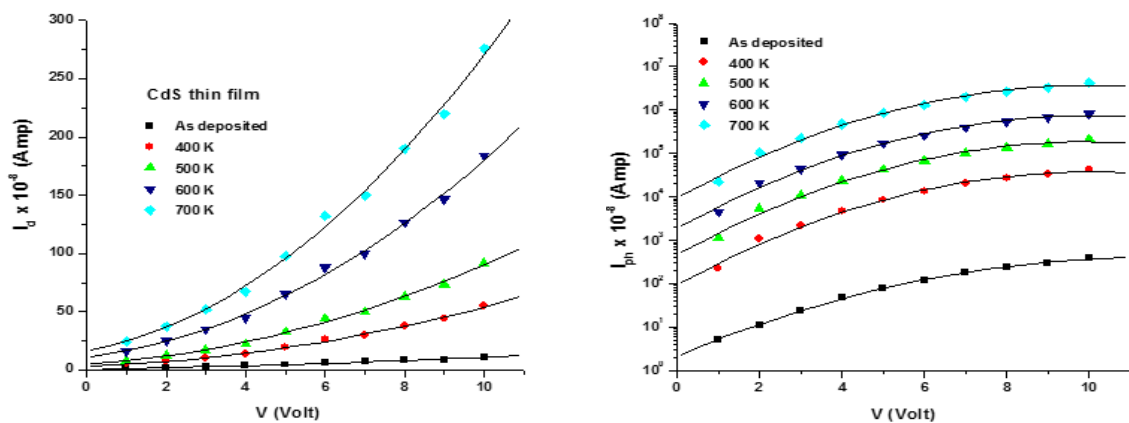
Fig. 10. The dark currents for photocurrents and against applied voltage of the as-deposited and annealed films.
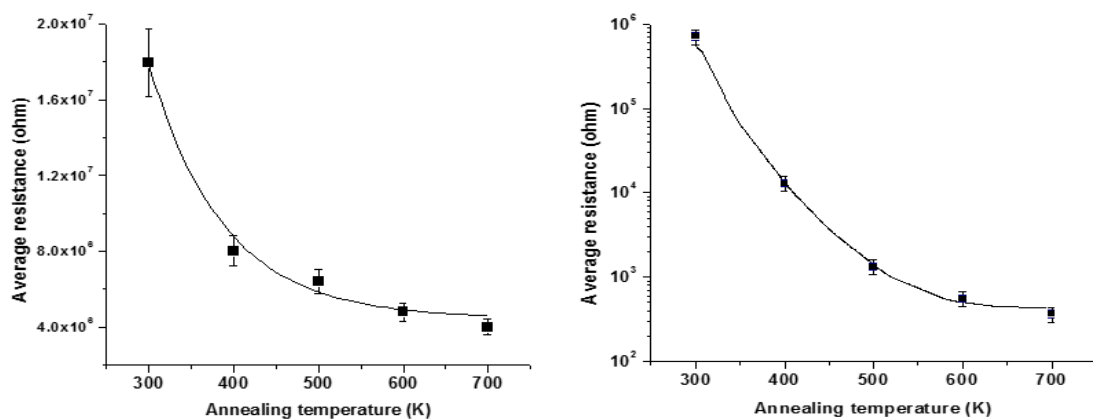
Fig. 11. The average resistance against annealing temperature for both dark and illumination of CdS thin films.

4. Conclusions

CdS films with a thickness of 500 nm were fabricated on glass substrates by a thermal evaporation technique. The effects of annealing temperature on CdS thin films were investigated at four different temperatures of 400, 500, 600 and 700 K in a nitrogen atmosphere. X-ray diffraction

patterns of the film displays that the peaks have cubic and hexagonal structure gradually convert to hexagonal with increasing the annealing temperature and predominantly hexagonal structure at 700 K. The crystallize size increases with increasing the annealing temperature while the lattice strain decreased. These behaviors were may be attributed to the improvement in the crystal structure of the film. The results indicate that the values of the refractive index are gradually decrease with increasing the annealing temperature. The allowed direct transition of CdS films is valid with band gap energy decreases from 2.45 to 2.24 eV. The current increases with increasing the annealing temperature overall values of applied voltage. Moreover, the photocurrent versus the applied voltage of each annealed film jump to higher values under the illumination.

References

[1] X. Mathew, J. P. Enriquez, A. Romeo, A. N. Tiwari, Sol. Energy **77**(6), 831 (2004).
[2] J. Han, C. Spanheimer, G. Haindl, G. Fu, V. Krishnakumar, J. Schaffner, C. Fan, K. Zhao, A. Klein, W. Jaegermann, Sol. Energy Mater. Sol. Cells **95**, 816 (2011).
[3] H. Kim, D. Kim, Sol. Energy Mater. Sol. Cells **67**(1–4), 297 (2001).
[4] N. Amin, K. Sopian, M. Konagai, Sol. Energy Mater. Sol. Cells **91**, 1202 (2007).
[5] L. Chu, A. Chu Shirley, Solid State Electron. **38**(1), 533 (1995).
[6] P. K. Nair, J. Campos, M. T. S. Nair, Semicond. Sci. Technol. **3**(2), 134 (1988).
[7] S. A. Mahmoud, A. A. Ibrahim, A. S. Riad, Thin Solid Films **372**, 144 (2000).
[8] S. A. Tomas, O. Vigil, J. J. Alvarado Gil, R. Lozada Morales, O. Zelaya Angel, H. Vargas, A. Ferreira da Silva, J. Appl. Phys. **78**(4), 2204 (1995).
[9] J. P. Enrique, X. Mathew, Sol. Energy Mater. Sol. Cells **76**, 313 (2003).
[10] P. K. Nair, J. Campos, M. T. S. Nair, Semicond. Sci. Technol. **3**(2), 134 (1988).
[11] R. Devi, P. K. Kalita, P. Purakayastha, B. K. Sarma, J. Optoelectron. Adv. M. **10**(11), 3077 (2008).
[12] F. Chen, W. Jie, X. Cai, Thin Solid Films **516**, 2823 (2008).
[13] J. N. Ximello-Quiebras, G. Contreras-Puente, J. Aguilar-Hernandez, G. Santana-Rodriguez, A. Arias-Carbajal Readigos, Sol. Energy Mater. Sol. Cells **82**, 263 (2004).
[14] B. R. Sankapal, R. S. Mane, C. D. Lokhande, Mater. Res. Bull. **35**, 177 (2000).
[15] H. Metin, R. Esen, J. Cryst. Growth **258**(1–2), 141 (2003).
[16] D. Patidar, N. S. Saxena, K. Sharma, T. P. Sharma, Optoelectron. Adv. Mat. **1**(7), 329 (2007).
[17] A. L. Patterson, Phys. Rev. **56**, 978 (1939).
[18] O. A. Fouad, S. A. Makhlouf, G. A. M. Ali, A. Y. El-Sayed, Mater. Chem. Phys. **128**, 70 (2011).
[19] K. Senthil, D. Mangalaraj, K. Narayandass, Appl. Surf. Sci. **169-170**, 476 (2001).
[20] D. Saikia, P. K. Gogoi, P. K. Saikia, Chalcogenide Lett. **7**(5), 317 (2010).
[21] H. Metin, M. Ari, S. Erat, S. Durmus, M. Bozoklu, A. Braun, J. Mater. Res. **25**(1), 189 (2010).
[22] E. R. Shaaban, J. Alloys Compd. **563**, 274 (2013).
[23] E. R. Shaaban, I. Kansal, S. Mohamed, J. M. Ferreira, Physica B: Condensed Matter. **404**, 3571 (2009).
[24] E. Szewczak, J. Paszula, A. V. Leonov, H. Matyja, Mater. Sci. Eng. A **226-228**, 115 (1997).
[25] M. El-Hagary, M. Emam-Ismail, E. R. Shaaban, A. Al-Rashidi, S. Althoyaib, Mater. Chem. Phys. **132**, 581(2012).
[26] M. A. Islam, M. S. Hossain, M. M. Aliyu, P. Chelvanathan, Q. Huda, M. R. Karim, K.

Sopian, N. Amin, Energy Proc. **33**, 203 (2013).

[27] H. Khallaf, C. T. Chen, L. B. Chang, O. Lupana, A. Dutta, H. Heinrich, A. Shenoud, L. Chow, Appl. Surf. Sci. **258**, 6069 (2012).

[28] Y. Wang, N. Herron, J. Phys. Chem. **95**, 525 (1991).

[29] E. R. Shaaban, A. Almohammedi, E. S. Yousef, G. A. M. Ali, K. F. Chong, A. Adel, A. Ashour, Optik, **164**, 527 (2018).

[30] Swanepoel, R.: Determination of the thickness and optical constants of amorphous silicon. J. Phys. E: Sci. Instrum., 16, 121 (1983)

[31] E. R. Shaaban, I. S. Yahia, E. G. El-Metwally, Acta Phys. Pol. A **121**, 628 (2012).

[32] P. K. Nair, M. T. S. Nair, J. Campos, L. E. Sansores, Sol. Energy Mater. **15**, 441 (1987).

[33] S. Kolhe, S. K. Kulkarni, M. G. Takwale, V. G. Bhide, Sol. Energy Mater. **13**, 203 (1986).